Polymer 49 (2008) 4826–4836

Contents lists available at ScienceDirect

Polymer

journal homepage: www.elsevier.com/locate/polymer

Properties of novel epoxy/clay nanocomposites prepared with a reactive phosphorus-containing organoclay

W.S. Wang, H.S. Chen, Y.W. Wu, T.Y. Tsai, Y.W. Chen-Yang*

Department of Chemistry and Center for Nanotechnology, Chung Yuan Christian University, 200 Chung-Pei Road, Chung-Li 32023, Taiwan, ROC

ARTICLE INFO

Article history:
Received 12 March 2008
Received in revised form 8 July 2008
Accepted 5 August 2008
Available online 15 August 2008

Keywords:
Epoxy
Clay
Nanocomposite

ABSTRACT

In this study, a reactive phosphorus-containing organoclay (RPC) was successfully prepared through the cationic exchange reaction of sodium montomorillonite clay with hexyltriphenylphosphonium bromide and surface modification by grafting it with glycidyloxypropyltrimethoxy silane. It is characterized using X-ray diffraction (XRD) and Fourier transform IR (FTIR) measurements. A series of novel epoxy/clay nanocomposites (ERPC) was then prepared with a selected epoxy resin and varying amounts of RPC. The results of XRD and TEM of the nanocomposites showed that the RPC particles were well dispersed in the epoxy matrix with a highly exfoliated structure due to the presence of the reactive epoxide group of RPC. The as-prepared epoxy/RPC nanocomposites (ERPC) were thermally stable up to 388 °C. Thermal stability was increased by increasing the RPC content as indicated by the corresponding activation energies (E_a) and the integral procedural decomposition temperatures (IPDT). Furthermore, the storage modulus in the glass state of the nanocomposites was dramatically increased with the increase in RPC content. In addition, the large increment of limiting oxygen index (LOI) which was 11 units higher than that of the neat epoxy indicates that an extraordinary enhancement of flame retardancy was obtained from the nanocomposite containing 5 wt% of RPC.

1. Introduction

Epoxy resins have been used in a variety of applications. For instance, they have been used as surface coatings and adhesives for electronics devices, and as structural reinforced composites for aerospace, marine vehicles, and automobiles. Although the advantage of the poly-functional reactivity of most epoxy systems leads to a high cross-linking density and meets the required matrix rigidity for applications, the brittleness and combustibility of these materials can be problematic and limit their potential applications. Additives or modifiers with inorganic fillers such as nano-powders, nano-tubes, and layered silicate clays [1–3] have been generally used to improve their physical and mechanical properties. Among these additives, layered silicate clays are particularly good candidates in improving the thermal, mechanical, barrier, and flame retardant properties of pure epoxy materials. These improvements are primarily a consequence of the interfacial effects that result from dispersing the silicate nanolayers in the polymer matrix and the high in-plane strength, stiffness, and aspect ratio of the lamellar nanoparticles. Epoxy/clay nanocomposites have been studied extensively in recent years [4]. However, the conventional technique usually resulted in an intercalated or intercalated/exfoliated structure rather than a well dispersed and highly exfoliated structure [5–7]. Since the dispersion and structure of the clay in the nanocomposites depend strongly on the extent of the compatibility between organic and inorganic phases, a significant amount of research has been carried out to improve the compatibility between clay and the polymer matrix [8–10].

In our previous study of PU/clay nanocomposites, we found that if the organophilic clay contains functional groups which can form chemical bonds with the polymer matrix, a very high degree of exfoliation of the clay platelets in the nanocomposite can be achieved, thereby enhancing the physical properties [11]. Furthermore, modification by grafting a proper functional organic silane into the hydroxyl groups present on the edge of the clay platelets has been found to be an efficient way to better disperse the clay in the polymer matrix via the reaction of the clay with the polymer matrix in the nanocomposites [12–14]. However, few of the epoxy/silane grafted clay nanocomposites have been reported [15,16].

In order to improve flame retardancy, thermal property, and mechanical property simultaneously, in this study, a reactive flame retardant clay (RPC) was synthesized from MMT using cationic exchange and grafting reactions. A series of the RPC-containing epoxy nanocomposites (ERPC) was then prepared in various

* Corresponding author. Tel.: +886 3 265 3317; fax: +886 3 265 3399.
E-mail address: yuiwhei@cycu.edu.tw (Y.W. Chen-Yang).

0032-3861/$ – see front matter © 2008 Elsevier Ltd. All rights reserved.
doi:10.1016/j.polymer.2008.08.019

contents of RPC. The microstructure, thermal mechanical behavior, and flame retardancy of the ERPCs were investigated. The thermal stabilities and kinetics of the thermal degradation of ERPCs were likewise studied.

2. Experimental

2.1. Materials

The sodium montmorillonite clay (MMT), PK802 with 116 meq/100 g of cation exchange capacity, was obtained from Pai Kong Industries, Taiwan. The modifier, hexyltriphenylphosphonium bromide (TP6), was prepared according to the method reported in Ref. [17]. Bisphenol A epoxy resin, EPON 828, was obtained from Polysciences, Inc. The curing agent, 4,4′-diaminodiphenylsulfone (DDS), was purchased from TCI Company. Glycidyloxypropyl-trimethoxy silane (GPMS) was obtained from Acros Organics Company. All the reagents were used as-received.

2.2. Preparation of the reactive phosphorus-containing flame retardant organoclay (RPC)

The reactive phosphorus-containing flame retardant organoclay (RPC) was prepared from the phosphorus-containing organoclay (POC) grafted with GPMS, an epoxide group-containing silane. POC was prepared using the cationic exchange reaction between MMT, PK802, and the modifier TP6 as reported previously [18]. Thus, 10.00 g of PK802 was stirred overnight in 1 L of distilled water at room temperature. A separate solution containing 4.83 g of TP6 in 500 mL of distilled water was kept under vigorous stirring. After stirring for 1 h, the modifier solution was added to the MMT suspension. The ion exchange reaction was then carried out by stirring the mixture for 24 h at 60 °C to obtain the organoclay. The organoclay was washed repeatedly with a fresh 2:1 mixture of de-ionized water and acetone. The POC powder was obtained by filtering out the solvents and freeze-drying the product. For the preparation of RPC, the procedure used for the ERPC-1 nano-composite, which contained 1 wt% of RPC, is described as an example. A stable suspension was obtained by suspending 0.0656 g of POC in acetone and stirring for 2 h. The suspension was then mixed with 0.00134 g of GPMS, which was calculated according to the formula reported [19] and stirred for 24 h at 60 °C to obtain the RPC solution. This solution was used directly in preparing the epoxy/RPC nanocomposite. In addition, to obtain the RPC powder for characterization, the solvent in the solution was filtered out, and the product was dried in an oven under a vacuum at 50 °C for 48 h.

The clays, MMT, POC, and RPC were characterized by FTIR spectra as shown in Fig. 1. The assignments of the absorptions are summarized as follows:

MMT: 3624 cm^{-1} (stretching of the structural hydroxyl group coordinated to octahedral atoms), 3468 cm^{-1} (H–OH of the hydrogen bonded water), 1641 cm^{-1} (O–H deformation of the entrapped water), 1110–1000 cm^{-1} (Si–O stretching), 915 cm^{-1} (Al–O/Al–OH stretching), 851 cm^{-1} (Al–MgOH deformation), 626 cm^{-1} (coupled Al–O and Si–O out-of-plane vibration), 522 cm^{-1} (Si–O–Al deformation) [20].

POC: for hexyltriphenylphosphonium unit 2933 and 2854 cm^{-1} (C–H stretching of hexyl group), 1486 cm^{-1} (C=C in plane stretching of the aromatic ring), 1440 cm^{-1} (C–H scissoring of P–CH_2–), 1120 and 748 cm^{-1} (P–Ph stretching), the characteristic absorptions of the structural tetrahedral and octahedral groups for layer silicates similar to MMT.

RPC: 2942 and 2841 cm^{-1} (C–H stretching of propyl group and Si–O–CH_3), 1254 cm^{-1} (C–O stretching of epoxide), 1200 cm^{-1} (C–H bending of propyl group), 1087 cm^{-1} (Si–O–CH_3 stretching), 907 and 820 cm^{-1} (ring vibration of epoxide group).

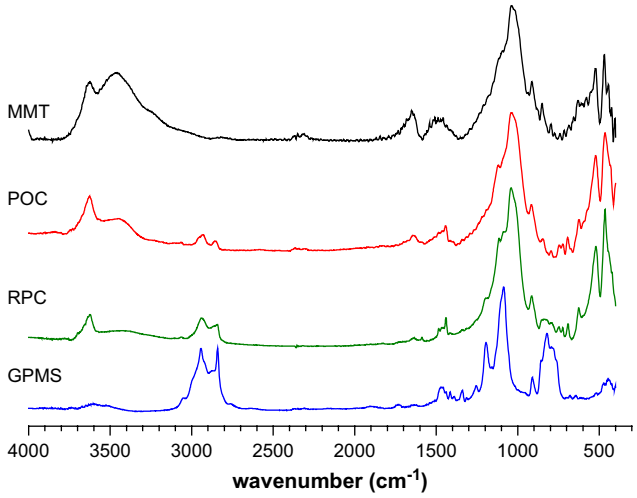

Fig. 1. FT-IR spectra of the pristine MMT and the organoclays.

2.3. Preparation of the epoxy/RPC nanocomposite

The synthesized reactive flame retardant organoclay RPC was used as the filler to prepare the epoxy/RPC nanocomposites. Thus, the RPC solution prepared above was mixed with the proper amount of epoxy resin and stirred for another 24 h. Then a stoichiometric amount of DDS based on the epoxide groups from both EPON 828 and GPMS was added to the mixture and stirred for 20 min. The mixture was sonicated for 1 h using an ultrasound bath by Delta D200H then poured into a mold; after which, the solvent was evaporated and degassed at 80 °C by vacuum. Finally, the mixture was cured for 1 h at 160 °C, 2 h at 225 °C, and 1 h at 235 °C to obtain the epoxy/RPC nanocomposites.

Moreover, in order to study the possible reaction between the epoxide groups on RPC and the curing agent DDS during the curing process, the test samples, ERPC-t and EGPMS-t, were prepared using the same procedure as for ERPC with the compositions listed in Table 1 and characterized by the FTIR measurement. Furthermore, for comparison, a series of the corresponding epoxy/POC nanocomposites (abbreviated as EPOC-*x*) was also prepared from the POC powder using the same procedure.

The fed compositions (or weight percentages) and abbreviations of the EPOC, ERPC and the test nanocomposites are listed in Tables 1 and 2.

2.4. Characterization

The microstructure and dispersion extent of the RPC particles in the epoxy matrix were investigated using a combination of wide angle X-ray diffraction (WXRD), Fourier transform infrared (FTIR) spectroscopy, and transmission electron microscopy (TEM). The WXRD measurement of the samples was performed on a PANalytical PW3040/60X' Pert pro (45 kV, 40 mA) diffractometer with

Table 1
Fed compositions of the EPOC-1, ERPC-1 and test sample composites

Sample	Epoxy (g)	DDS (g)	POC (g)	RPC (g)	GPMS grafted on RPC (g)	POC used for RPC (g)	GPMS (g)
EPOC-1	5.00	1.65	0.07	–	–	–	–
ERPC-1	5.00	1.65	–	0.07	0.0013	0.0656	–
ERPC-t	2.50	0.84	–	2.50	0.0500	2.4500	–
EGPMS-t	2.50	1.65	–	–	–	–	3.14

Table 2
Compositions, abbreviations, TGA and DMA data of the EPOC and ERPC nanocomposites

Sample	Organoclay	Weight percentage of organoclay (wt%)	IDT (°C)	T_{max} (°C)		Char yield at 800 °C (%)	Storage modulus at 100 °C (MPa)	T_g (°C)
				1st	2nd			
Neat Epoxy	–	0	395	419	581	0.44	1263	219
EPOC-1	POC	1	388	407	581	1.17	1547	219
EPOC-3	POC	3	388	403	586	3.44	1702	218
EPOC-5	POC	5	386	403	567	5.47	1846	212
ERPC-1	RPC	1	396	422	658	1.00	1583	211
ERPC-3	RPC	3	393	424	675	2.10	1735	212
ERPC-5	RPC	5	394	421	661	3.40	1874	216

a copper target ($\lambda = 1.54$ Å) and a scanning rate of 4°/min from 2° to 40°. The clay samples for the measurements were compression packed powders and were aligned perpendicular to the diffraction axis. The FTIR spectra were obtained using a JASCO FTIR-4200 spectrometer with KBr pellets for solid specimens. The TEM micrographs were taken with a JEOL-JEM 2010 TEM apparatus at 200 kV in bright field mode. The samples were microtomed into the 80 nm-thick thin sections using a Leica ultra-microtome with a diamond knife and collected on 200 mesh copper grids.

The fractured surface morphologies of the nanocomposites were examined using a field emission scanning electron microscopy (FE-SEM) (Hitachi S-4100, Japan) instrument. The specimens were slightly cracked with a thin razor blade and then fractured with a hammer. Before examination, all the samples were adhered onto the adhesive carbon tapes supported by a circular metallic disk. The samples were coated with platinum using a sputter coater to avoid charging.

The tensile strength tests were performed using the material testing machine HT-9102M (Hungta Instrument Co., Ltd., Taiwan) according to ASTM D638 standard. The specimens used had dimensions of $150 \times 15 \times 2$ mm^3, and the test speed was 1 mm/min.

The thermogravimetric analysis (TGA) and derivative thermogravimetry (DTG) of the clays and composites were performed using a TA Instruments Q50 under air atmosphere at a flow rate of 60 mL/min. The samples were heated from 40 to 800 °C at a heating rate of 20 °C/min. The initial degradation temperature (IDT) was determined as the temperature at which 5 wt% weight loss ($T_{5\%}$) occurred, and the temperatures at maximum rate of weight loss (T_{max}) were taken from the peak values of the differential thermogravimetric thermograms.

The storage modulus and glass transition temperature (T_g) of the nanocomposites were measured with dynamic mechanical analysis (DMA) by TA Instruments Q800. The size of the specimens was $8 \times 14 \times 2$ mm^3. The sample was clamped in a medium frame using a small center clamp in the dual cantilever mode. The analyses were performed at a frequency of 1 Hz and a temperature range of 40–250 °C at a heating rate of 3 °C/min. The T_g value was taken to be the temperature at the maximum of the tan δ peak.

The flammabilities of the nanocomposites were evaluated in terms of limiting oxygen index (LOI) by the equipment made according to ASTM D 2863 standard [21]. The LOI value measures the minimum oxygen concentration (in a flowing mixture of oxygen–nitrogen gas) required to support candle-like downward flame combustion under the specific conditions for about 3 min prior to extinguishing. The specimens used for the test had a dimension of $100 \times 6 \times 3$ mm^3. The gas was allowed to flow for 30 s to purge the system before the test. The specimen was ignited so that entire tip was burning. The relative flammability was determined by adjusting the concentration of oxygen which permitted the specimen to burn. The LOI value was then calculated from the following formula [22]:

$$\mathrm{LOI} = \frac{V_o \times 100}{V_o + V_N}$$

where V_o represents the volumetric flow of oxygen and V_N represents the volumetric flow of nitrogen.

3. Results and discussion

3.1. Characterization of the organoclays

Fig. 2 shows the WXRD patterns of MMT, POC, and RPC. As can be seen, the $d_{(001)}$ peak of MMT and POC is observed at $2\theta = 7.00°$ and $2\theta = 4.65°$, respectively. From the values, the corresponding d-spacings of MMT and POC are 1.2 nm and 1.9 nm, respectively. This indicates that the galleries of the silicate layers in MMT had been expanded for about 0.70 nm by the phosphonium ions. The diffraction pattern of RPC, obtained from POC modified with GPMS, indicates that the $d_{(001)}$ peak at $2\theta = 4.68°$, corresponding to 1.88 nm interlayer spacing, is almost the same as that of POC. This implies that the modification of the epoxide-containing silane group only had a minimal effect on the intrinsic intercalated structure of the clay. This means that the GPMS molecules modified mostly the surface and edges of the POC clay sheets as indicated in Scheme 1. The possible reason is that the interlayer spacings of POC were filled with phosphonium ions, which hindered the diffusion of the GPMS molecules into the galleries of clay sheets to react with the hydroxyl groups within as reported [23,24].

The thermal analysis of the clays was also investigated by TGA and DTG measurements. As shown in Fig. 3, the thermogram of MMT indicates three steps of weight loss, in which the first step (4.87%, below 100 °C) corresponds to the loss of water absorbed on the MMT particle surface, the second step corresponds to the gradual loss of the interlayer water in MMT (4.99%, 400–650 °C), and the third step corresponds to the dehydroxylation of MMT (3.36%, 650–800 °C) and the inorganic residue of 86.70% at 900 °C. The thermogram of POC exhibits fewer loss of water (0.57%) at a temperature lower than that of MMT, implying that less water is absorbed in POC than in MMT. This confirms the increase in the hydrophobic property of POC due to the hydrophobicity of the exchanged phosphonium ions. The thermogram observed between 200 and 500 °C accounts for 26.4% of the overall weight loss, which involves a three-step decomposition process of the organic fragments of the phosphonium group. The maximum rate loss of the

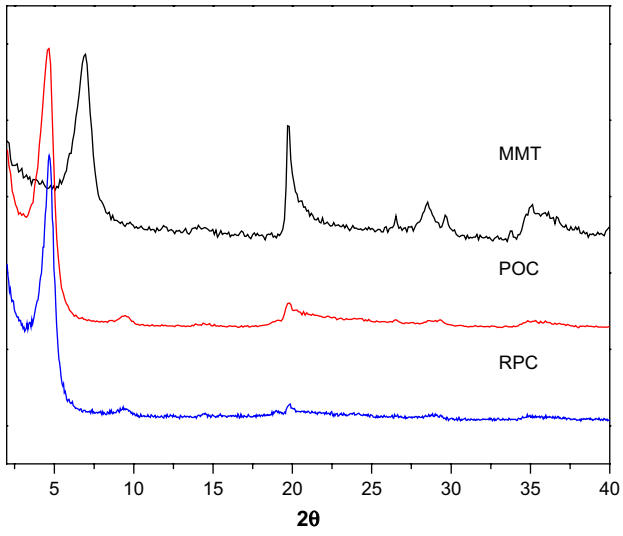

Fig. 2. XRD diffraction patterns of the pristine MMT and the organoclays.

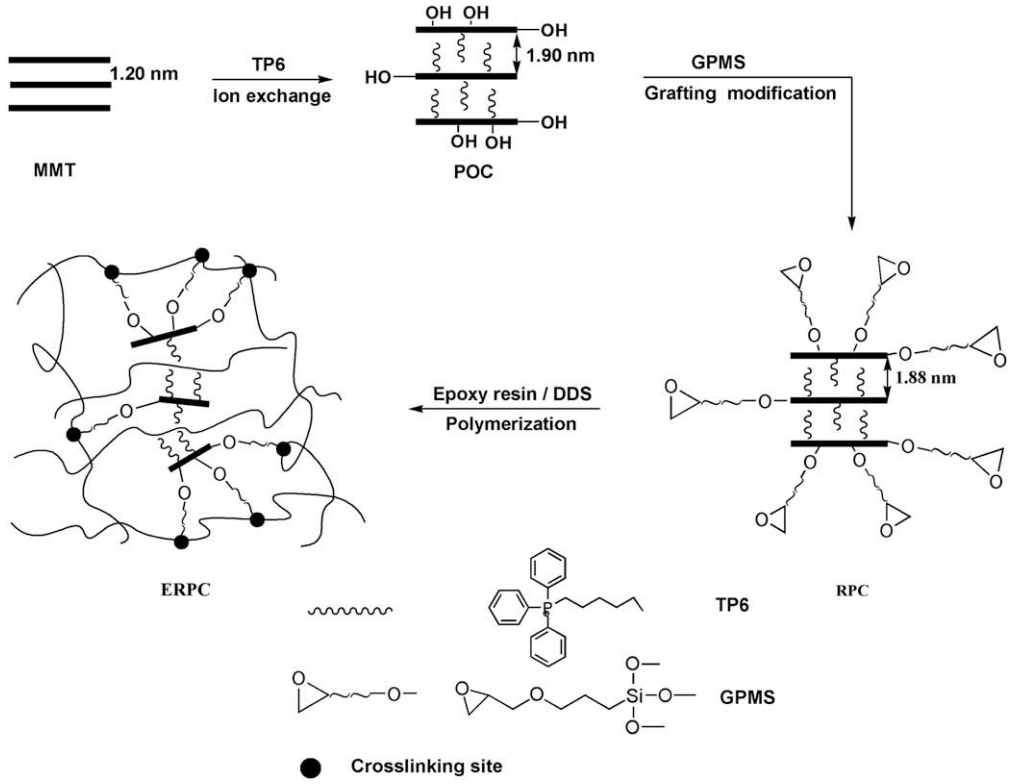

Scheme 1. Possible change in silicate layers structure of RPC during the preparation of RPC and ERPC.

interlayer water in POC occurred at about 610 °C, which is close to that for MMT. This is ascribed to the similar ordered silicate structure. However, the dehydroxylation that occurred at a temperature (~690 °C) lower than that in MMT is due to the larger *d*-spacing in POC as revealed by the WXRD result. Moreover, the inorganic residue that remained at 900 °C was decreased to 65.20%. Similar to that of POC, the DTG curve of RPC exhibits that the loss of adsorbed water (3.55%) and the loss of interlayer water occurred below 100 °C and 610 °C, respectively, and the dehydroxylation took place at 690 °C. It is noticed that the decomposition of the organic fragments, including the silane and phosphonium groups, occurred at a temperature higher than that of POC and peaked at 433 °C with lesser weight loss (13.35%), causing the higher inorganic residue to remain at 900 °C. The result indicates that RPC has higher thermal stability than POC. This higher thermal stability of RPC may be due to the enhanced hindered effect of the highly exfoliated silicate layers of RPC on the diffusion of oxygen and volatile products throughout the composite materials.

3.2. Characterization of the nanocomposites

Fig. 4(a) shows the WXRD patterns of the neat epoxy and epoxy/POC nanocomposites containing 1, 3, and 5 wt% of POC (EPOC-*x*, $x = 1, 3, 5$). In Fig. 4(a), two broad diffraction peaks at about 5.00° and 18.00° are observed for the neat epoxy. The diffraction peak (001) of POC overlapping with the lower angle broad peak of the epoxy matrix is observed at around 4.60° for EPOC-1. It reveals that the *d*-spacing of the silicate layers in EPOC-1 was not expanded further by the epoxy polymer but was rather reduced from 2.67 nm to 1.92 nm. This is ascribed to the high curing temperature, which favored extragallery polymerization than intragallery polymerization for the in situ curing process of the epoxy/POC composites as explained in other studies [25,26]. Furthermore, the peak at the same angle is observed for EPOC-3 and EPOC-5, and the intensity was increased by increasing the POC loading. This indicates that basically, no epoxy resin intercalated into the silicate layers in all the EPOC-*x* nanocomposites, and the ordered structure remained with a smaller *d*-spacing than that of pure POC. On the other hand, Fig. 4(b) shows the XRD diffraction patterns of the neat epoxy and epoxy/RPC nanocomposites (ERPC-*x*) containing 1–5 wt% of RPC. We can see that unlike that of the EPOC-*x* nanocomposites, the diffraction patterns of the ERPC-*x* nanocomposites do not exhibit any diffraction peak in the range of 2–10° angles. This implies that the *d*-spacings of the RPC layers were expanded further in the as-prepared ERPC-*x* nanocomposites and were larger than the XRD detection limit of 4.41 nm. The RPC silicate layers were very much delaminated or possibly became a complete exfoliation structure. This also implies that the presence of the reactive epoxide group on the surface/edge of RPC provided the active sites for reacting with the curing agent. This resulted in the silicate layers being delaminated and the *d*-spacings expanding [13]. The complete disappearance of the broad peak at $2\theta = 5.00°$, a diffraction of the neat epoxy, indicates that the order of the epoxy network was depressed due to the presence of the well-dispersed RPC platelets that might have participated in the curing process by interacting with DDS. The crystalline phase of the epoxy matrix was changed to the clay–platelets-interacted phase [27]. This is also ascribed to the proper dispersion of RPC in the epoxy matrix caused by the covalent bonds formed between RPC and DDS and cross-linked with the epoxy matrix. This result is similar to that found in the PU/clay nanocomposites we prepared previously wherein a covalent bond was also formed between the clay and the polymer matrix [11].

3.3. FTIR spectroscopy

The amount of RPC added in the ERPCs was less than 5 wt%, so the reaction between RPC and DDS was not easy to investigate from their FTIR spectra. In order to confirm that the epoxide groups on RPC did participate in the curing process of ERPC, the FTIR spectra

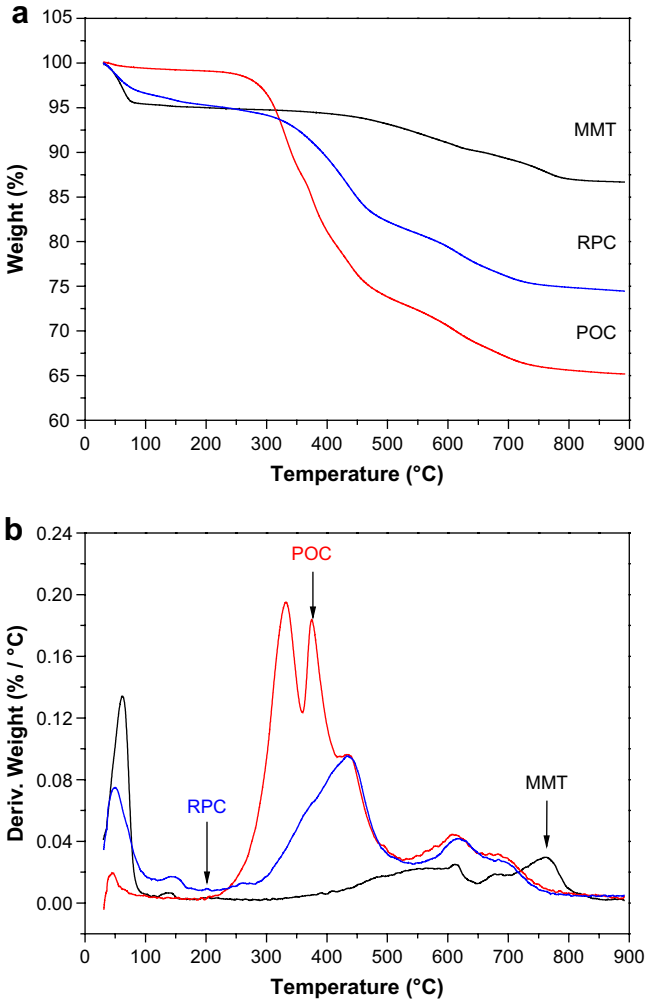

Fig. 3. Thermogravimetric analysis plots of the clays. (a) TGA curves (b) DTG curves.

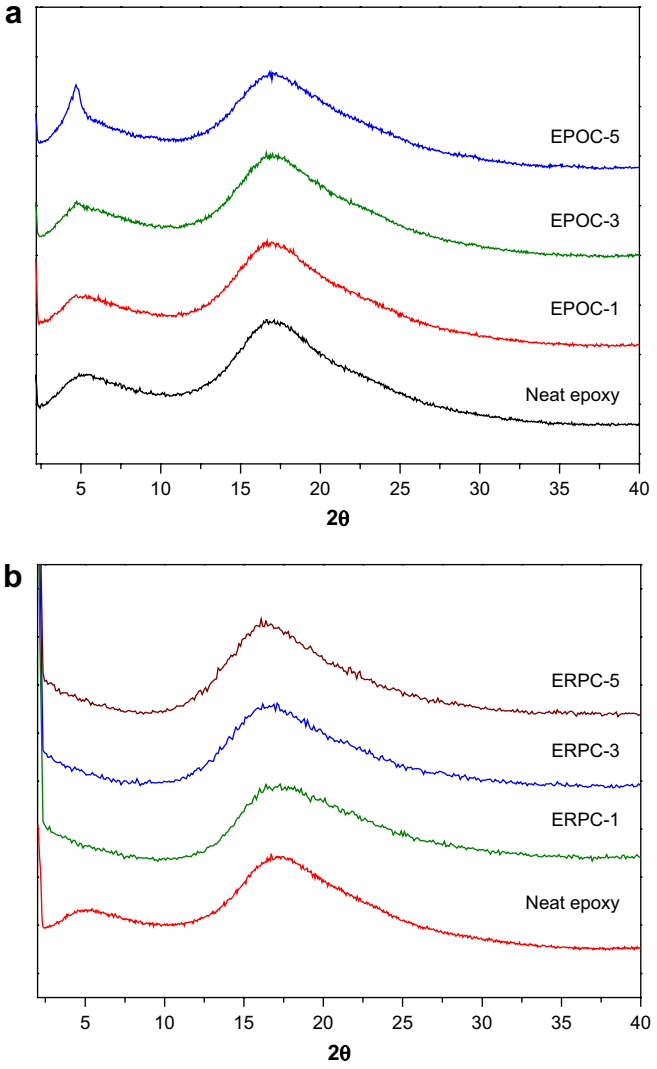

Fig. 4. XRD diffraction patterns of the nanocomposites (a) EPOC-*x* (b) ERPC-*x*.

of the test samples, namely, ERPC-t which was prepared with a much higher amount of RPC than ERPC-*x*, and EGPMS-t which was prepared with GPMS, were measured before and after the curing process. As can be seen in Fig. 5(a), before curing, the characteristic absorptions were observed at 3368 and 3242 cm^{-1} for the N–H stretching of the amine group and 1630 cm^{-1} for the N–H bending of the primary amine of DDS, and at 3050 and 907 cm^{-1} for the asymmetric C–H stretching and ring vibration of the epoxide groups. After curing, Fig. 5(b) shows that the N–H stretching and N–H bending vibration absorptions from DDS and the absorptions of C–H stretching and ring vibration of the epoxide groups disappeared, while an extra absorption peak at 1365 cm^{-1} corresponding to the C–N stretching of the tertiary amine, formed by curing, was observed. This indicates that not only the epoxide groups from epoxy resin but also that from GPMS was reacted with DDS. On the other hand, in Fig. 5(c), the FTIR spectra of ERPC-t show that before curing, the other features were all similar to those shown in Fig. 5(a) as expected, except that the Si–O–Si stretching absorption of silicate between 1000 and 1100 cm^{-1} was overlapped with the Si–O–R absorption of the silane group. Furthermore, after curing, Fig. 5(d) also shows similar spectrum feature for the cured ERPC-t as Fig. 5(b) for the cured EGPMS-t. This result suggests that the added RPC did react with DDS during the preparation of the ERPC nanocomposites.

The results also demonstrate that the clay layers in the ERPCs were capable of being pulled apart/shifted away from the ordered structure through the reaction of the epoxide groups on the surface/edge of RPC and the amines of DDS. The latter also reacted with the epoxide groups of the epoxy resin, such that the silicate layers were highly exfoliated and were well dispersed among the epoxy matrix as a cross-linked matrix in ERPC. From the results of the WXRD and FTIR measurements, the possible change in the silicate layers structure of RPC during the preparation of ERPC is depicted in Scheme 1.

3.4. Morphology

The morphologies of the nanocomposites were examined using TEM and SEM measurements. The representative TEM images of EPOC are shown in Fig. 6(a) with different magnifications. The image with lower magnification (left figure) indicates that the POC particles were aggregated in the epoxy matrix, and the particle sizes were in sub-μm-scale. The image with higher magnification (right figure), the dark lines, which correspond to the intersection of clay platelets in EPOC-3, confirms that the POC clay platelets were in ordered tactoid structure in the epoxy matrix as initially revealed by the WXRD pattern discussed above. The ordered structure illustrates that the polymer chains hardly intercalated into the silicate galleries due to the favored extragallery polymerization in the high-temperature curing process. Fig. 6(b) shows the

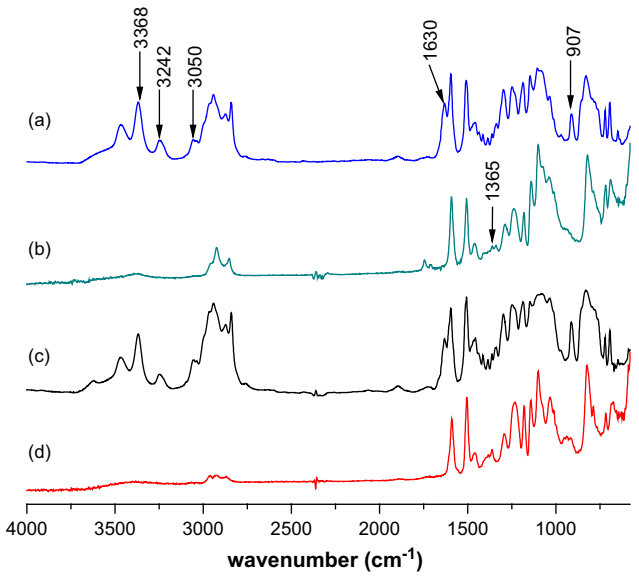

Fig. 5. FT-IR spectra of ERPC-t (a) before curing (b) after curing and EGPMS-t (c) before curing (d) after curing.

TEM micrographs of the nanocomposite samples with 5 wt% RPC, ERPC-5. As can be seen in the image with lower magnification (left figure), the clay platelets were homogeneously and randomly dispersed in the epoxy matrix. Moreover, the basal spacings of the clay nanoplatelets in the epoxy matrix can be easily distinguished. In the image with higher magnification (right figure), it is further shown that the expanded *d*-spacing of the separated silicate platelets in the nanocomposites was less than 20 nm, and the thickness of the single platelet was about 1 nm. In comparison with EPOC-3 which exhibited only about 2–3 nm spacing of the primary intercalated stack in Fig. 6(a), the layered silicate platelets of RPC were much more effectively delaminated in the epoxy matrix than that of POC. This also reveals that the silicate platelets of RPC were in a very highly exfoliated structure in the epoxy matrix due to the presence of the epoxide groups grafted on the surface/edge of the clay platelets, which participated in the curing process, pulling apart/shifting away the silicate platelets from the ordered structure.

Fig. 7 shows the SEM micrographs of the fractured surfaces of the neat epoxy, EPOC-5, and ERPC-5 nanocomposites. As shown in Fig. 7(a), the cleavage surface of the neat epoxy is quite smooth, and the crack propagation lines are almost parallel to one another and can hardly be seen. This indicates that the neat epoxy is quite brittle as expected. The micrographs of the EPOC nanocomposites in Fig. 7(b) show fractured flakes with cleavage borders, indicating that the interface between POC and the epoxy matrix was weak and easily broken by force. This can be attributed to the poor compatibility between the aggregated POC particles and the epoxy matrix. On the other hand, Fig. 7(c) shows that the fractured surfaces of the ERPC nanocomposites were rough without any river-like crack and fractured flakes, revealing that the material was not as brittle as the neat epoxy; the interfaces between RPC and the epoxy matrix were also rather invisible. This result also supports the fact that the RPC clay platelets were homogeneously and finely dispersed in the epoxy matrix as evidenced from the TEM images, and that the interaction between the clay and the epoxy matrix did occur during the polymerization.

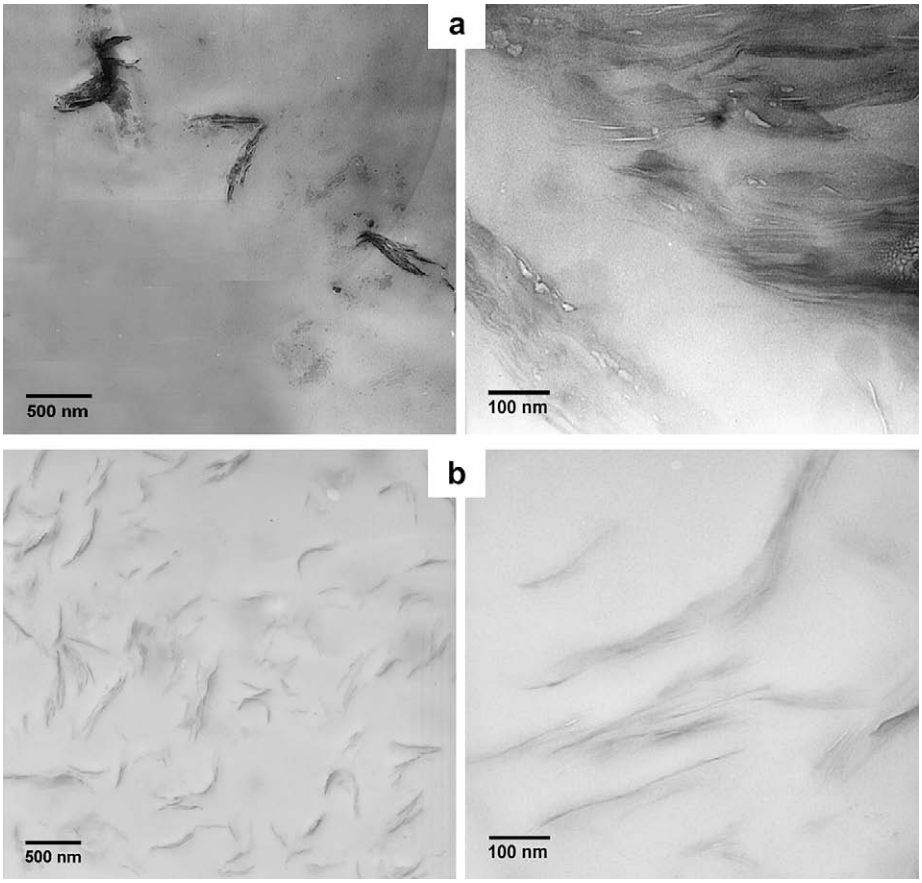

Fig. 6. The TEM images of (a) EPOC-3 (b) ERPC-5.

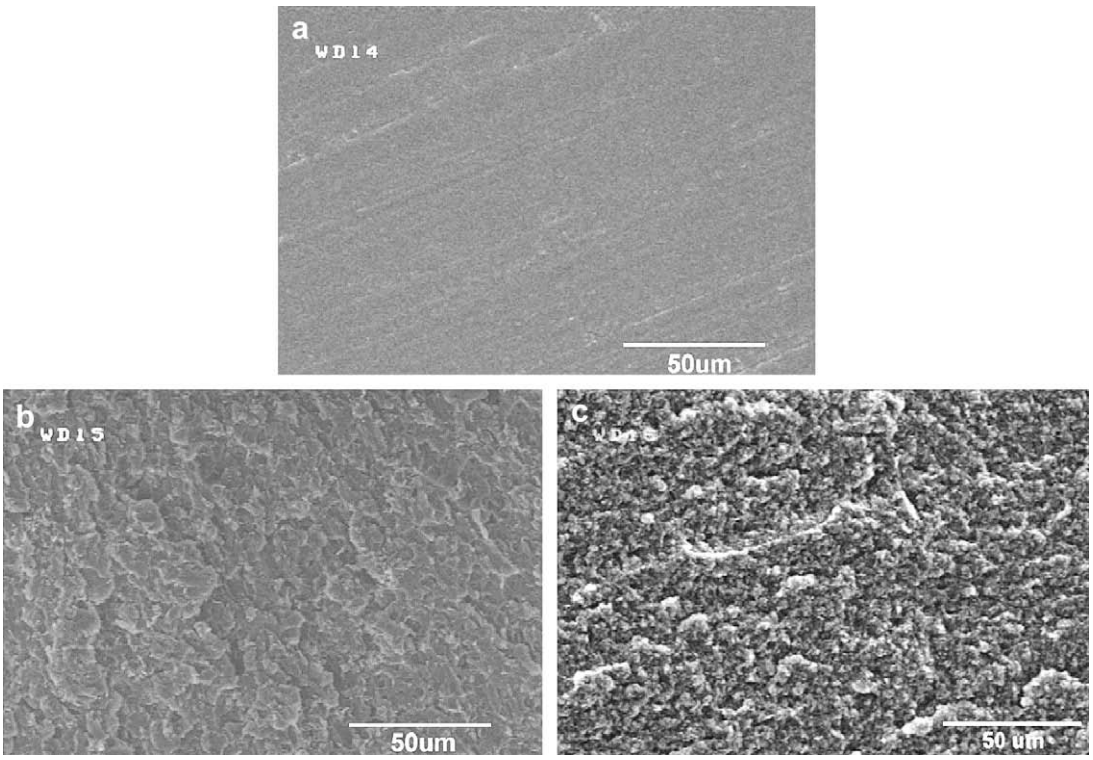

Fig. 7. Fracture surface SEM images of (a) neat epoxy (b) EPOC-5 (c) ERPC-5.

3.5. Thermal stability

The thermal properties of the as-prepared nanocomposites were investigated using TGA measurements. Fig. 8 shows the TGA thermograms of the neat epoxy, EPOC, and ERPC nanocomposites in air. The corresponding data are listed with the data of EPOC (the thermograms are not shown) in Table 2. It is found that the initial degradation temperature (IDT) of EPOC in air was lower than that of neat epoxy (395 °C) and remained similar with the increase in POC loading (from 388 °C to 386 °C). Meanwhile, the IDTs of ERPCs were almost the same as those of neat epoxy. This result indicates that ERPCs possessed better thermal stability than EPOCs. The neat epoxy thermally degraded in air through a double-step process with maximum rate at 414 and 581 °C. It is believed that the main loss (~70%) in the first stage was due to the degradation of the epoxy network structure, leaving about 30% of char residue which was further thermally oxidative degraded in the second stage. This resulted in zero residue at a temperature higher than 700 °C [28].

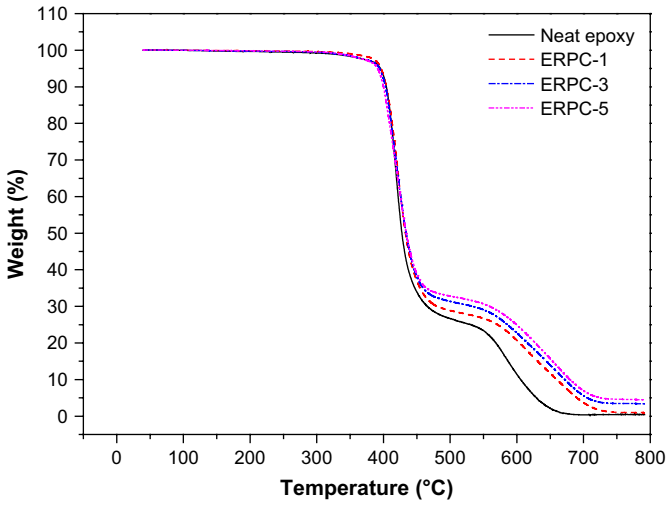

Fig. 8. TGA thermograms of neat epoxy and ERPC-*x* in air.

The maximum degradation temperatures, T_{max}, of the EPOC nanocomposites were slightly lower than those of neat epoxy but were all higher than 400 °C and slightly varied with the POC loading. However, as can be seen in Fig. 8, the T_{max}s of ERPCs were all obviously higher than those of neat epoxy. This reveals that the EPOC nanocomposites were less stable than the neat epoxy, which is attributed to the lesser stability of the phosphonium groups in POC as shown in Fig. 3(a). This is consistent with the previous results reported [29,30] as well as with the decrease in cross-linking density of the epoxy resin caused by the presence of the organoclay [31]. On the other hand, the ERPC nanocomposites were more stable than the EPOC nanocomposites and neat epoxy. This is ascribed to the higher thermal stability of RPC than POC as indicated in Fig. 3(b), the enhancement in the compatibility of RPC with epoxy resin due to the presence of RPC's organic portions, and the extra cross-linking due to the presence of the epoxide groups of RPC which participated in the curing process as discussed above. Furthermore, the char yields of the composites at about 450 °C were all higher than those of neat epoxy. This is attributed to the formation of char by the silicate layers and phosphonium part of the clays, retarding the degradation in the second stage. The residues for EPOC-5 and ERPC-5 at 800 °C corresponded to the remaining inorganic parts of the clays as indicated in Fig. 3(a).

3.6. Kinetics of thermal degradation

The thermal stability of a material is usually characterized by the initial degradation temperature and degradation rate, which are both related to activation energy. Therefore, the determination of the degradation's activation energy is necessary to better understand the thermal stability of the material. The kinetics of thermal degradations of several epoxy-based nanocomposites has been

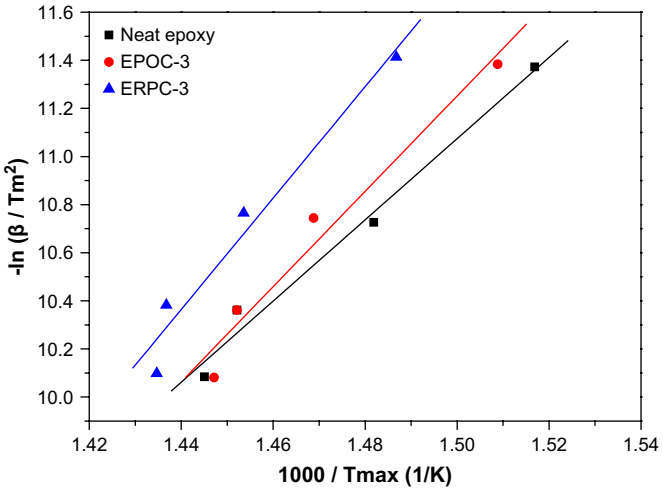

Fig. 9. Kinetics of the thermal degradation of EPOC-3 and ERPC-3 as evaluated by the Kissinger equation in air.

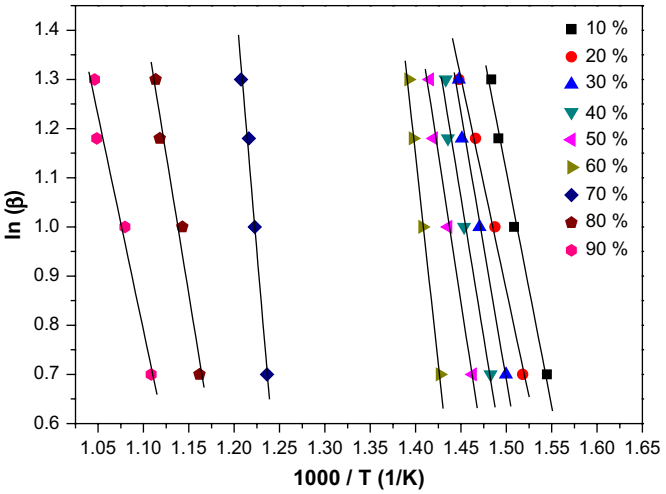

Fig. 10. Kinetics of the thermal degradation of ERPC-3 as evaluated by the Flynn–Wall–Ozawa equation in air.

studied by analyzing TGA curves with different methods [32,33]. The results all indicated that if the added clay layers were in a higher degree of exfoliation structure, the activation energies of the degradation of the composites would increase with the increase in clay loading. In this study, the well-known Kissinger equation and Flynn–Wall–Ozawa method were used to evaluate the thermal degradation activation energy of the EPOC and EPRC composites.

The Kissinger equation in its linear form is shown below [34]:

$$\ln\left(\frac{\beta}{T_{\max}^2}\right) = \left\{\ln\frac{AR}{E} + \ln\left[n(1-\alpha_{\max})^{n-1}\right]\right\} - \frac{E_a}{RT_{\max}} \quad (1)$$

where β, T, and R are the heating rate, absolute temperature, and gas constant, respectively. $T_{\max}$ is the temperature at the maximum rate of weight loss, A is the pre-exponential factor, $\alpha_{\max}$ is the extent of conversion at $T_{\max}$, and n is the reaction order. Accordingly, the activation energy (E_a) of the individual sample was obtained from the slope of the plot of $\ln(\beta/T^2_{\max})$ versus $1/T_{\max}$, which was fitted to a linear equation. The representative plots of the first degradation stage of neat epoxy, EPOC-3, and ERPC-3 are shown in Fig. 9. The corresponding E_a values of the EPOC-x and ERPC-x systems are summarized in Table 3. We can see that the E_a values of the first degradation stage for all the nanocomposites were higher than those of neat epoxy. They were largely increased by 34% and 55% for EPOC-5 and ERPC-5 with an increase in organoclay loading of up to 5 wt%. The same was the case for the second degradation stage which increased by 61% and 77% for EPOC-5 and ERPC-5, respectively.

The results imply that although the clay layers of POC were in ordered tactoids structure as mentioned above, they still exhibited a retarding effect on the degradation of EPOC-x. This is attributed to the good thermal resistance of the clay particles dispersed in the nanocomposites, thereby resulting in the increase of energy required for the degradation. Besides, the E_a value of each ERPC-x sample was higher than that of the corresponding EPOC-x sample with the same clay loading. This reveals that the activation energy of the thermal degradation also depended on the degree of delamination of the clay layers in the epoxy matrix. Furthermore, the higher the degree of delamination, the larger the activation energy as previously reported [32,33].

On the other hand, the Flynn–Wall–Ozawa method is based on mass losses in different degradation regions during the thermal degradation process. The method is evaluated according to the following equation [34]:

$$\log(\beta) = \log\frac{AE}{Rg(\alpha)} - 2.315 - \frac{0.457E_a}{RT} \quad (2)$$

where β, T, α, and R are the heating rate, the absolute temperature to reach the conversion, the degree of conversion, and the gas constant, respectively. For this equation, E_a can be calculated based on the slope of a plot of $\log(\beta)$ versus $1/T$ for fixed values conversion (α). Fig. 10 plots $\log\beta$ versus $1/T$ for ERPC-3 at 9 conversions, and the dependence of E_a on α for neat epoxy, EPOC-3, and ERPC-3 is shown in Fig. 11. It can be seen that the activation energies were

Table 3
Thermal stability and kinetics data of the EPOC and ERPC composites

Sample	Activation energy evaluated by Kissinger method E_a (kJ/mol)		IPDT (°C)	LOI
	1st	2nd		
Neat epoxy	140	96	259	23
EPOC-1	150	116	265	25
EPOC-3	164	142	274	26
EPOC-5	187	156	293	26
ERPC-1	180	129	281	29
ERPC-3	192	152	301	32
ERPC-5	218	172	302	34

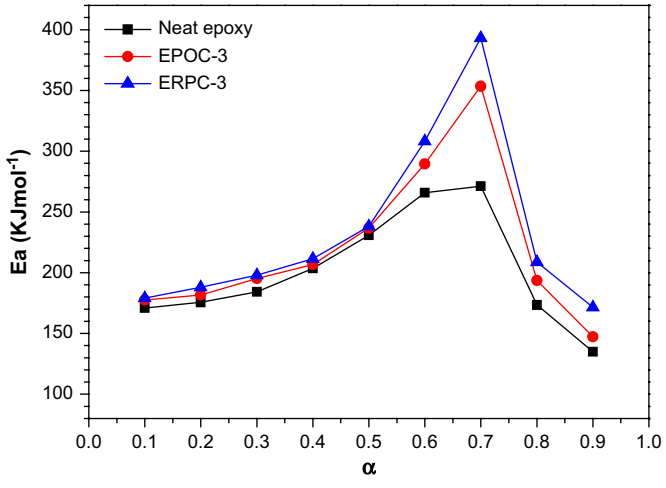

Fig. 11. Plots of activation energy with various conversions by the Flynn–Wall–Ozawa equation method.

increased with an increase in α value, and they reached maximum at $\alpha = 0.7$, which corresponded to the end of the first degradation stage and the formation of the char yield. As indicated, the E_a values of EPOC-3 and ERPC-3 were similar and only slightly higher than those of neat epoxy in the lower α value range (<0.5). However, the α value was higher than 0.5, so the activation energy of the composites was significantly higher than that of neat epoxy. Furthermore, the E_a value of ERPC-3 was obviously higher than that of EPOC-3, revealing a higher effect in the enhancement of thermal stability for ERPC-3 than EPOC-3 as found from the Kissinger method.

In addition, an investigation for the nanocomposites is carried out by evaluating the integral procedure decomposition temperature (IPDT), a thermal stability factor of the nanocomposite, which is correlated to the volatile parts of the polymeric materials, as proposed by Doyle [35]. IPDT is determined on the basis of the overall shape of the TGA curve, so it can estimate the overall inherent thermal stability for the decomposition proceeded in a single or several consecutive steps.

A schematic diagram of a typical TGA thermogram revealing the areas of A1, A2, and A3 is shown in Fig. 12 for the determination of IPDT. The value of IPDT is calculated as follows [32]:

$$\mathrm{IPDT} = [(\mathrm{A1} + \mathrm{A2})^3/\mathrm{A1}(\mathrm{A1} + \mathrm{A2} + \mathrm{A3})^2](T_f - T_i) + T_i \quad (2)$$

where T_i and T_f are the beginning-of-test temperature and the end-of-test temperature of the TGA measurement, respectively. The IPDT values calculated for the cured resins are summarized in Table 3. As can be seen, the IPDT value increased with an increasing organoclay loading. With the addition of 5 wt% of the organoclay, an increase in IPDT value was observed for both EPOC-5 and ERPC-5 as compared to neat epoxy. The IPDT value of neat epoxy was 259, while that of EPOC-5 and ERPC-5 was 293 and 302, respectively. The increments are attributed to the organoclays POC and RPC in the epoxy matrix, which contributed retardant effects to the heat and oxygen spreading and the char formation during the heating process. The IPDT values of the ERPC-*x* composites were also all larger than those of the corresponding EPOC-*x* composites due to the better dispersion and higher degree of exfoliation of the clay layers of RPC than that of POC in the epoxy matrix. The results are consistent with their activation energies and confirm that the epoxide-containing silane groups grafted on the organic clay resulted in a homogeneous epoxy/clay hybrid material during the thermal curing process.

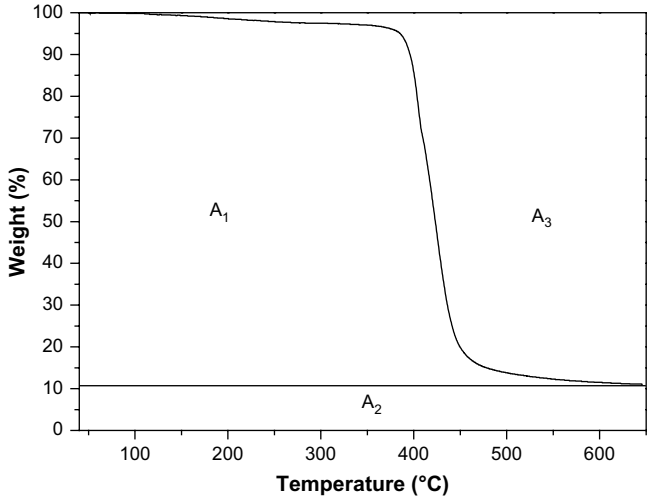

Fig. 12. Schematic diagram of Doyle's method for determining IPDT.

The enhancement is ascribed to the presence of well-dispersed and highly exfoliated clay layers that acted as an insulator and mass transport barrier for the volatile products generated during the degradation. Moreover, the interaction between the clay and epoxy resin, resulting in an exfoliated clay layer structure and the extra cross-linking in the nanocomposites, is also an important factor.

3.7. Flame retardant properties

The dispersed silicate layers of clay in the nanocomposites can serve as good barriers against gases such as oxygen, nitrogen, and decomposed vapors by insulating the underlying materials and slowing down the rate of mass loss of the degraded products; in addition, the char residue formed in the high-temperature range can protect oxygen diffusion [22,36]. Thus, it is anticipated that the flame retardancy of the highly exfoliated flame retardant organoclay-containing ERPC-*x* nanocomposite would be largely enhanced. Therefore, the limiting oxygen indices (LOIs) of the nanocomposites were evaluated. As listed in Table 3, the LOI value of EPOC-1 was higher than that of neat epoxy for about 2 units, but it did not increase as the POC content was further increased. This may be ascribed to the aggregation of the POC particles which reduced the surface area. On the other hand, the LOI value of ERPC-*x* was higher than that of EPOC-*x* and largely increased with the increase in RPC content. When 1 wt% of RPC was added, the LOI of ERPC-1 increased from 23 to 29, and as the RPC loading was increased to 5 wt%, as high as 34 of the LOI value or an increase of 11 units was obtained for ERPC-5. This reveals that the flame retardant efficiency of RPC in the epoxy matrix was additive due to the good dispersion of RPC in the epoxy matrix and the high surface area caused by its highly exfoliated structure. Overall, the improvement in flame retardancy is mainly ascribed to the synergistic effect of the phosphonium ions and silicates in the clay, but other factors such as the combination of delayed mass loss from the clay nanocomposite and the possibility that the phosphorus structure is a vapor phase flame retardant may be also at work.

3.8. Tensile mechanical properties

The tensile mechanical properties of neat epoxy, EPOC-5, and ERPC-5 are summarized in Table 4. It is shown that neat epoxy had the smallest elongation, 4.4%, and showed brittle characteristic. Compared with that of neat epoxy, the tensile strength, yield strength, elongation at break, and modulus of EPOC-5 were increased at 37%, 187%, 54%, and 10%, respectively. On the other hand, 56%, 285%, 61%, and 39% increases in the tensile strength, yield strength, elongation at break, and modulus, respectively, are found for ERPC-5. The more enhanced tensile mechanical properties of ERPC-5 are mainly attributed to the better dispersion and higher exfoliation of the silicate layers in ERPC-5, which were cross-linked with the epoxy matrix through the epoxide groups of RPC. The result is consistent with the SEM micrographs discussed above.

3.9. Thermal dynamic mechanical analysis

Fig. 13(a) illustrates the DMA plots of storage modulus (E') versus temperature for ERPC nanocomposites as a function of clay

Table 4
Mechanical properties of the neat epoxy, EPOC-5 and ERPC-5 nanocomposites

Sample	Modulus (MPa)	Tensile strength (MPa)	Yield strength (MPa)	Elongation (%)
Neat Epoxy	575	33.9	12.4	4.4
EPOC-5	634	46.6	35.6	6.7
ERPC-5	799	53.1	47.7	7.0

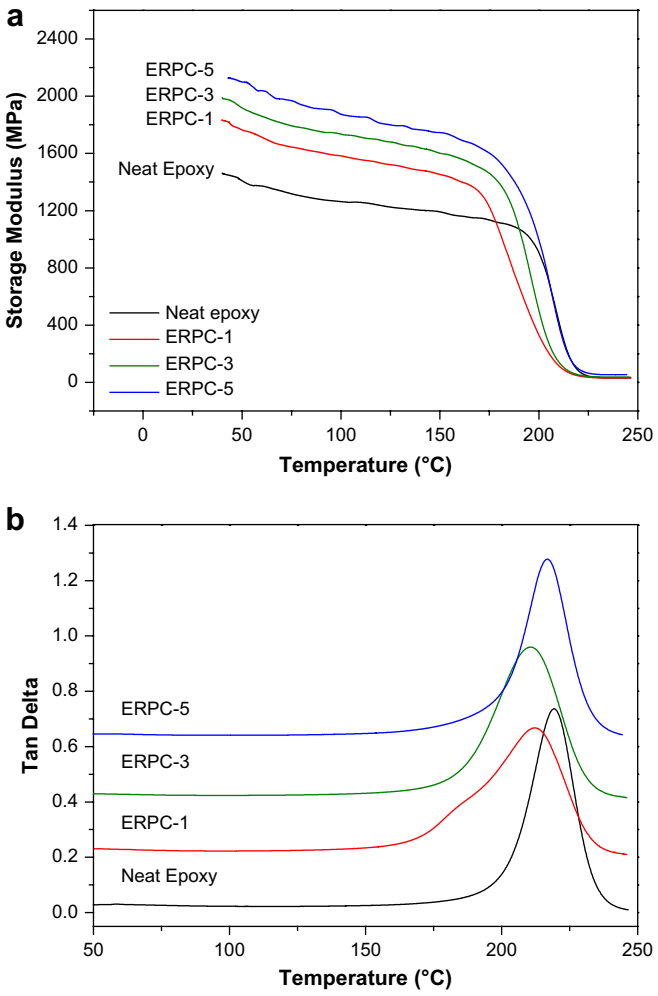

Fig. 13. DMA plots of neat epoxy and the ERPC nanocomposites.

concentration. As summarized in Table 2, the E' values of the ERPC-x samples in the low-temperature region (the glassy region) are higher than those of neat epoxy. This indicates that the storage modulus in the glass state of the epoxy matrix was effectively improved due to the addition of RPC. For comparison, the corresponding E' values at 100 °C for the EPOC system are also listed in Table 2. It can be seen that as the organoclay content increases to 5 wt%, the storage modulus steadily increases by 46% (from 1263 to 1846 MPa) and 48% (from 1263 to 1874 MPa) for EPOC-5 and ERPC-5, respectively. The enhancement is attributed to the presence of organoclay particles. The larger enhancement of E' value for the ERPC system than the EPOC system is attributed to the better dispersion of the reactive RPC than POC in the epoxy matrix as observed in the TEM images.

As shown in Fig. 13(b) and Table 2, the T_g value of EPOC-x obtained from the DMA measurements was similar to that of neat epoxy. This indicates that when the content of POC was low, the hindrance of the un-reactive clay particles was not large enough to disturb the movement of the epoxy chain. This was due to the poor dispersion of the clay particles and the high cross-linking of the epoxy matrix as revealed by the high T_g. However, as the content was increased to 5 wt%, the T_g of EPOC-5 was lowered significantly [22], indicating that the cross-linking of the epoxy was significantly hindered by the presence of more POC clay particles. This in turn resulted in the reduction of the epoxy matrix's cross-linking density and an increase in the movement of the polymer chain. On the other hand, the T_g value of ERPC-1 was significantly lower than that of neat epoxy. This is attributed to the good dispersion of the silicate layers of RPC in the epoxy matrix, which more effectively hindered the cross-linking of the epoxy matrix than that of POC. As a result, there was easier movement of the polymer chain. Nevertheless, as the content of the reactive RPC was increased, T_g was increased accordingly. This is attributed to the increase in cross-linking densities through the formation of the extra cross-linking between RPC and the epoxy matrix. This was caused by the reaction of the reactive epoxide groups on the surface/edge of RPC and DDS. In other words, the extra cross-linking offset the diminishing of the cross-linking among epoxy resin, which was caused by the hindrance of the silicate platelets.

4. Conclusions

In this study, a reactive flame retardant phosphorus-containing organoclay (RPC) was prepared by the cationic exchange reaction of the sodium montomorillonite clay with hexyltriphenylphosphonium bromide to form the organoclay (POC). This was followed by surface modification with the grafting of glycidyloxypropyltrimethoxy silane. The epoxy/POC (EPOC-x) and epoxy/RPC (ERPC-x) nanocomposites with different clay concentrations were prepared by using POC and RPC as the filler, respectively.

The results of the WXRD, TEM, and FE-SEM measurements of the ERPC-x nanocomposites showed that the RPC organoclay was much better dispersed and higher exfoliated in the epoxy matrix than the POC organoclay. This was attributed to the participation of RPC in the polymerization process. The FTIR, The TGA thermograms showed that all the nanocomposites were still thermally stable up to 388 °C. The IPDT of the nanocomposite was increased with an increase in organoclay content, revealing the increase in stability of the nanocomposites in the whole temperature range measured. On the other hand, the activation energy value was increased with an increase in the organoclay content up to 5 wt%, confirming the increase in thermal stability of the nanocomposites at the fast decomposition stage. The LOI values of the nanocomposite indicated that the flame retardancy of the epoxy was tremendously enhanced by the addition of the organoclays. The LOI value was largely increased from 23 to 34 for ERPC-5, which was 9 units higher than that of the corresponding EPOC-5. The storage modulus of the ERPC nanocomposite at 100 °C in the glass state was steadily increased with the increase in organoclay content and was higher than that of the corresponding EPOC nanocomposite. Overall, the addition of organoclay on the epoxy properties had a more profound effect in the ERPC system than in the EPOC system. This is attributed to the better dispersion and higher exfoliation of RPC in the epoxy matrix than POC, which is caused by the presence of the reactive epoxide groups that participated in the polymerization.

Acknowledgement

The authors would like to thank National Science Council of ROC (NSC 92-2745-M-033-001) and Chung Yuan Christian University of Taiwan, ROC (CYCU-95-CR-CH) for financially supporting this research work. Our gratitude also goes to Prof. Shyh-Shin Hwang of the Department of Mechanical Engineering of Ching Yun University for his assistance in the tensile mechanical test.

References

[1] Yu HJ, Wang L, Shi Q, Jiang GH, Zhao ZR, Dong XC. Prog Org Coat 2006;55:296.
[2] Ye Y, Chen H, Wu J, Ye L. Polymer 2007;48:6426.
[3] Kint DPR, Seeley G, Gio-Batta M, Burgess AN. J Macromol Sci Part B Phys 2005;44:1021.
[4] Ray SS, Okamoto M. Prog Polym Sci 2003;28:1539.
[5] Zerda AS, Lesser AJ. J Polym Sci Part B Polym Phys 2001;39:1137.
[6] Miyagawa H, Drzal LT, Carsello JA. Polym Eng Sci 2006;46:452.

[7] Qi B, Zhang QX, Bannister M, Mai YW. Compos Struct 2006;75:514.
[8] Lin CH, Feng CC, Hwang TY. Eur Polym J 2007;43:725.
[9] Yang Y, Wu D, Li C, Liu L, Cheng X, Zhao H. Polymer 2006;47:7374.
[10] Abdalla M, Dean D, Adibempe D, Nyairo E, Robinson P, Thompson G. Polymer 2007;48:5662.
[11] Chen-Yang YW, Lee YK, Chen YT, Wu JC. Polymer 2007;48:2969.
[12] Lu H, Hu Y, Li M, Chen Z, Fan W. Compos Sci Technol 2006;66:3035.
[13] Sen S, Sa MM, Nugay N, Nugay T. Polym Int 2006;55:216.
[14] Leu CM, Wu ZW, Wei KH. Chem Mater 2002;14:3016.
[15] Ha SR, Rhee KY, Kim HC, Kim JT. Colloid Surf A 2008;313–314:112.
[16] Ha SR, Ryu SH, Park SJ, Rhee KY. Mater Sci Eng A 2007;448:264.
[17] Douat C, Heitz A, Paris M, Martinez J, Fehrentz JA. J Pept Sci 2002;8:601.
[18] Chen-Yang YW, Wang WS, Tang JC, Wu YW, Chen HS. J Mater Res 2008;23:1618.
[19] Gültek A, Seçkin T, Önal Y, İçduygu MG. Turk J Chem 2002;26:925.
[20] Katti KS, Sikdar D, Katti DR, Ghosh P, Verma D. Polymer 2006;47:403.
[21] ASTM Committee E-5. ASTM fire test standards. 3rd ed. ASTM; 1990. p. 278–82.
[22] Ratna D, Chakraborty BC, Dutta H, Banthia AK. Polym Eng Sci 2006;46:1667.
[23] Qian X, Liao M, Zhang W. Polym Int 2007;56:399.
[24] Chen GX, Kim HS, Yoon JS. Polym Int 2007;56:1159.
[25] Camino G, Tartaglione G, Frache A, Manferti C, Costa G. Polym Degrad Stab 2005;90:354.
[26] Oh TK, Hassan M, Beatty C, El-Shall H. J Appl Polym Sci 2006;100:3465.
[27] Jan IN, Lee TM, Chiou KC, Lin JJ. Ind Eng Chem Res 2005;44:2086.
[28] Zammarano M, Franceschi M, Bellayer S, Gilman JW. Polymer 2005;46:9314.
[29] Liu YL, Wang YH, Chen HS. Macromol Chem Phys 2005;206:600.
[30] Schartel B, Knoll U, Hartwig A, Pütz D. Polym Adv Technol 2006;17:281.
[31] Gu A, Liang G. Polym Degrad Stab 2003;80:383.
[32] Guo B, Jia D, Cai C. Eur Polym J 2004;40:1743.
[33] Brnardić I, Macan J, Ivanković H, Ivanković M. J Appl Polym Sci 2008;107:1932.
[34] Kim HS, Chen GX, Jin HJ, Yoon JS. Colloids Surf A 2008;313–314:56.
[35] Dolye CD. Anal Chem 1961;33:77.
[36] Liu YL, Hsiue GH, Chiu YS, Jeng RJ, Perng LH. J Appl Polym Sci 1996;61:613.